Fibottention: Inceptive Visual Representation Learning with Diverse Attention Across Heads

Ali Khaleghi Rahimian[1]   Manish Kumar Govind[1]   Subhajit Maity[2]   Dominick Reilly[1]
Christian Kümmerle[1†]   Srijan Das[1†]   Aritra Dutta[2†]
[1]UNC Charlotte   [2]UCF
{akhalegh, kuemmerle, sdas24}@charlotte.edu   aritra.dutta@ucf.edu
† Equal contribution as Project Lead

Abstract

Visual perception tasks are predominantly solved by Vision Transformer (ViT) architectures, which, despite their effectiveness, encounter a computational bottleneck due to the quadratic complexity of computing self-attention. This inefficiency is largely due to the self-attention heads capturing redundant token interactions, reflecting inherent redundancy within visual data. Many works have aimed to reduce the computational complexity of self-attention in ViTs, leading to the development of efficient and sparse transformer architectures. In this paper, viewing through the efficiency lens, we realized that introducing any sparse self-attention strategy in ViTs can keep the computational overhead low. Still, these strategies are sub-optimal as they often fail to capture fine-grained visual details. This observation leads us to propose a general, efficient, sparse architecture, named Fibottention, for approximating self-attention with superlinear complexity that is built upon Fibonacci sequences. The key strategies in Fibottention include: it *excludes proximate tokens* to reduce redundancy, employs *structured sparsity* by design to decrease computational demands, and incorporates *inception-like* diversity across attention heads. This diversity ensures the capture of complementary information through non-overlapping token interactions, optimizing both performance and resource utilization in ViTs for visual representation learning. We embed our Fibottention mechanism into multiple state-of-the-art transformer architectures dedicated to visual tasks. Leveraging only 2-6% of the elements in the self-attention heads, Fibottention in conjunction with ViT and its variants, consistently achieves significant performance boosts compared to standard ViTs in nine datasets across three domains — image classification, video understanding, and robot learning tasks. We have made the code publicly available at https://github.com/Charlotte-CharMLab/Fibottention.

1   Introduction

We are in an era of transformer-based architectures (large foundation models, *e.g.* , GPT [43, 44, 7], BERT [19], ALBERT [34], ViT [21], DETR [8], D-DETR [71], CLIP [29], *etc.*) and they overwhelm the success of other DNN architectures in many downstream tasks such as object detection and tracking [22], document summarizing [43], language modeling [19], video understanding [47], and protein folding, to name a few. Transformers' performance comes at the expense of training them on a large corpus of high-quality data and extraordinary computational scale. *E.g.*, the smallest variant of the recent large language model, Llama-3 [2] has 8B parameters; it requires 32GB GPU memory to load and 64GB GPU memory to train with state-of-the-art training protocols. With their fast adoption in AI and the rapid advancement of technology, there has been a growing research interest in

developing *efficient transformers* that can be deployed and trained effectively on diverse edge devices or the Internet of Things (IoT) [1, 46, 57, 42].

At the core of the transformer-based architectures are the layers consisting of multi-head self-attention (MHSA) [30, 58, 21], in which the input data, $X \in \mathbb{R}^{N \times d}$ in the form of N input tokens, each in a d-dimensional embedding space [4], are mapped via learnable ($d \times d$) parameter matrices, or the so-called query, key and value matrices, $Q, K, V \in \mathbb{R}^{N \times d}$. After splitting Q, K, V column-wise into h equal-sized blocks, $\{Q_i\}_{i=1}^h, \{K_i\}_{i=1}^h, \{V_i\}_{i=1}^h \subset \mathbb{R}^{N \times d/h}$ also known as *heads*, the computational bottleneck of such layers lies in computing and processing the unnormalized self-attention matrices, $A_i = Q_i K_i^\top / \sqrt{d_h}$ with $d_h = d/h$ [58, 21], which consists of $N \times N$ scaled dot products between rows of Q_i and K_i, respectively. The vanilla vision transformer (ViT) [21] architecture is inspired by the transformer encoder [58]. Given an input image, $X \in \mathbb{R}^{H \times W \times C}$ of resolution $H \times W$, ViT use $p \times p$ patches to generate $N = \frac{HW}{p^2}$ tokens; see Figure 1(a).

Long input sequences characterized by large N contribute to the transformer's success and pose quadratic computational overhead, $O(N^2)$ in calculating the self-attention. To harvest efficiency, one of the popular approaches involves observing the attention matrices A_i only at a sparse subset of their entries $\Omega \subset [N] \times [N]$ of size $s = |\Omega| < N^2$ [12, 67, 5, 68, 49]. However, the quest for finding suitable choices for such support sets, Ω, with a favorable trade-off between efficacy and efficiency, is difficult due to data, model, and instance dependence of the attention weights and their sparsity patterns. Popular sparse attention strategies include local attention with sliding windows of fixed window size [61, 5, 45], in which only interactions between tokens that are spatially close to each other and random attention [68, 70] are considered; [10] uses a certain neighborhood which resembles diagonal sliding of a window, [5] uses dilated window. The first wave of works [5, 67, 66, 68] propose to approximate the attention matrix A by a *structured sparse matrix*. Surprisingly, except a few works [69, 70], attempts to design efficient transformers in the visual domain (such as the vision transformers [21, 56]) catered to specific needs of visual representation tasks, remained relatively unaffected by these trends in the language research community.

In this paper, our pursuit of designing an efficient self-attention mechanism for visual tasks is a combination of the knowledge translations from the NLP domain and our experience in dissecting self-attention mechanisms for visual tasks. We gained the following key insights: (*i*) *the principal diagonal* in A is indeed the least important due to the presence of redundant information in pixel space; that (*ii*) *structured sparsity* (non-random) is desirable and the other efficient sparse designs [68, 49] that include different sub and super-diagonals entries in the attention matrix are essential as they capture different token to token interactions; that (*iii*) *inception-like* diversity [53] across the attention heads are important; and finally, (*iv*) visual tasks are vastly different from language tasks; although not desired, vision tasks can account for underlying dataset biases (e.g., classification tasks and video understanding tasks are prone to different dataset biases), and therefore, *low overlap between attention heads* is optimal.

Taken together, in this work, we propose a dilated sliding windowed strategy to extract local-level token information at different scales in different heads that effectively boost performance on visual tasks and can be incorporated into any attention mechanism. First, we propose general sparse support selection mechanism (§3.1) that is equipped with two hyperparameters: (*a*) a *dilation sequence* $(f_n)_n \subset \mathbb{N}$, which determines the sequence of distances between indices of tokens in A that attend to each other, and (*b*) a *window size*, $1 \le w \le N$, for a given attention head, A. Building on this general mechanism, we propose Fibottention — where the dilation sequence is chosen to be the Fibonacci sequence (§3.2) with a moderate computational complexity of $O(N \log N)$. Fibottention can be used in conjunction with state-of-the-art transformer architectures catered for visual representation tasks — vanilla ViT (base and tiny) [21], CVT base [63], Swin transformer [37], and TimesFormer [6].

We extensively evaluate the proposed Fibottention on a diverse set of vision tasks (§4). Our findings indicate that ViT employing our proposed Fibottention outperform their baselines by up to +9.4%, +81%, +6.1% in image classification, video action classification, and robot imitation learning, respectively. This improvement is achieved by performing only about **2-6%** of local interactions of key-query pairs for computing self-attention. Furthermore, our efficient Fibottention can be integrated into any existing vision transformer without significantly compromising performance.

2 Related Work

Adapted from transformers [58] with capabilities of long-range sequencing modeling, vision transformer (ViT) [21] emerged as a popular architecture in visual understanding tasks. While ViTs [21, 56] particularly thrived in outperforming their traditional counterparts in visual representation tasks, these architectures suffer from large computational requirements, which is a well-known problem for the transformers intended for large-scale datasets [54].

The primary goal of efficient self-attention design is to find the *best approximation* of $QK^\top$ at the expense of reduced total FLOPs (importantly, reducing the quadratic dependence on N) compared to the original self-attention. The above problem is similar to *a structured sparse recovery problem*, where the original matrix $QK^\top$ is approximated by a sparse matrix $\mathcal{C}(QK^\top)$ which needs to have a typical structure attributed to capture the effect of the original matrix, here the self-attention. Yun et al. [67] showed that by maintaining a certain sparsity pattern, a sparse attention model can universally approximate any sequence-to-sequence function.

In that attempt, the first generation of papers postulates that diagonal elements in the attention map and their neighboring inner products of tokens are important [13, 32]. We also note that several directions have been explored towards sparsification of attention matrix [15], either indirectly by low-rank approximation [28, 60] or directly using selective sampling strategies [68]. In NLP, a multitude of works [25, 68, 5] concluded the necessity of global-scale token interaction [32] and local-level regional token interactions [32, 35] which resembles diagonal sliding of window [68] or dilated window [5] in the attention matrix for robust representation learning. In summary, Longformer [5], BigBird [68], ETC [3], Star-Transformer [25] use some variants of a local, global, sliding window, dilated sliding window and random attention pattern; see Figure 1-(b). In the second generation of papers, by using a differentiable search, Shi et al. [50] observed that diagonal elements, containing the interactions of each token to itself in the self-attention, $QK^\top$ to be redundant and unnecessary, and proposed to learn a differentiable attention mask. However, this structured sparsity is less explored in ViTs, where the data is highly redundant and contextually distinct from the language domain. ViTs [21, 56], leaned towards knowledge distillation [64], token pruning and merging [37], neighborhood attention [27], etc. among the most prominent strategies. The search for better ViT [56] architectures using the replication of global and local (window-based) token interaction is explored by the use of convolutions either directly [70] or indirectly [69] inducing regional inductive bias similar to existing hybrid vision transformer architectures [17, 63]. However, these architectures exhibit lower throughput and lack the robustness of ViTs in processing multiple modalities [24].

Adaptive and Dynamic Attention. A few works have considered non-uniform sparse attention patterns. [62] proposed unstructured, learned, instance-dependent attention masks. There is a limited number of works studying varying attention masks or support sets across attention heads. E.g., [32] noted that the performance of transformer models can be improved by disabling attention for a subset of heads. Although Longformer [5] discusses the exploration of different attention masks for various heads in MHSA and dilated window attention techniques have been investigated in NLP, these operations have not been explicitly explored in their adaptation for vision applications [69]. In the vision domain, SparseViT [11] implements sparsity-aware adaptation to efficiently find the optimal layerwise sparsity configuration (or pruning) for different layers. Recently, iFormer [51] proposed layers that mix local-level information at different frequency ranges by including convolution modules as parallel heads which rely exclusively on versions masked MHSA to achieve an *inception-like* effect [53]. In contrast, we focus on developing convolution-free architecture to retain its robustness.

3 Methodology: Diverse Sparse Attention and Fibottention

Shi et al. [50] empirically observed that diagonal elements in the self-attention, $QK^\top$ are the least important. Motivated by this observation, and with the notion of efficiency in mind, we design an architecture that dispenses the diagonal elements and a (variable) band of entries across the diagonals from each head. Instead, our architecture facilitates a variable dilation of the window in each head and captures different sub and super-diagonals of the attention matrix.

3.1 Sparse Attention with Windowed Dilation Sequences

In the following, we provide a general sparse attention framework that allows formulating and comparing different sparsity patterns for attention heads $\{A_i\}_{i=1}^h$. In particular, instead of observing the attention matrix A_i at each of its N^2 entries, we compute only the dot products whose indices are supported on a subset $\Omega \subset \{1, 2, \ldots, N\}^2$, i.e., we can define the sparse attention matrix
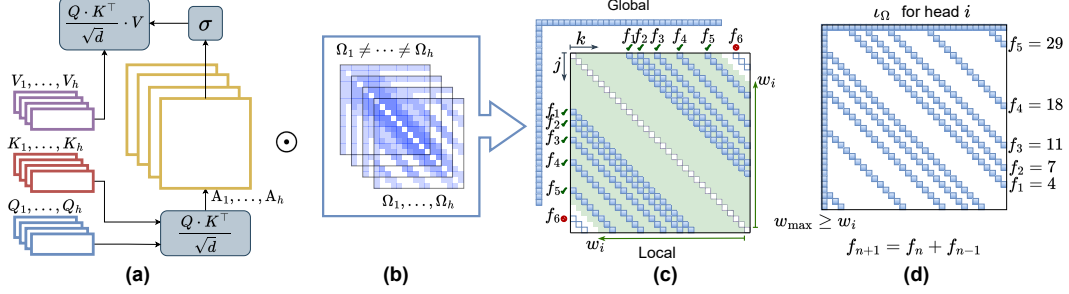
Figure 1: (a) The multi-head self-attention. (b) A general sparse attention computation strategy. A sequence of sparse support sets, $\{\Omega_i\}_{i=1}^h$, where each set selects $|\Omega| < N^2$ entries of the attention matrix. (c) The generalized masking strategy of Fibottention that controls sparsity of each attention matrix A_i through a dilated sequence, $(f_n)_n \subset \mathbb{N}$, and a fixed window size, w for each head. (d) An example of Fibottention.

$A_i^\Omega \in \mathbb{R}^{N \times N}$ of the i-th head corresponding to mask Ω as

$$(A_i^\Omega)_{j,k} = \begin{cases} \frac{Q_i^{(j)\top} K_i^{(k)}}{\sqrt{d_h}}, & \text{if } (j,k) \in \Omega, \\ -\infty, & \text{if } (j,k) \notin \Omega; \end{cases} \tag{1}$$

for any $j, k \in [N]$, where $Q_i^{(j)} \in \mathbb{R}^{d_h}$ and $K_i^{(k)} \in \mathbb{R}^{d_h}$ are the j-th query vector and the k-th key vector of the i-th attention head, respectively. If $\odot$ denotes the entrywise matrix multiplication, also called Hadamard product, this can be written as $A_i^\Omega = \text{sign}(A_i) \odot (|A_i| \odot \iota_\Omega)$, where $\iota_\Omega \in \mathbb{R}^{N \times N}$ is an indicator matrix of the index set Ω that is 1 for indices $(j,k) \in \Omega$ and $-\infty$, otherwise. In this work, we study structured support sets that capture both local and global interactions while ensuring efficient inference and training through sparsity. To this end, we introduce the notion of a *dilation sequence*, $(f_n)_n \subset \mathbb{N}$, which determines the sequence of distances between indices of tokens that attend to each other. Furthermore, for a given attention head, we fix a *window size*, $1 \leq w \leq N$, which, independently of the dilation sequence, provides an upper bound for the index distance between interacting token indices in an attention matrix.

Given the sequence, $(f_n)_n$ and parameter, w, we define the *support set*, $\Omega_w^{(f_n)}$ of *interacting query-key pairs dilated by* $(f_n)_n$ *of window size* w such that

$$\Omega_w^{(f_n)} = \big\{ (j,k) : |j - k| \in \{f_n\}_n, |j - k| \leq w \big\} \subset \{1, 2, \dots, N\}^2.$$

We refer to Figure 1-(c) for visualizing such support sets; $\Omega = \Omega_w^{\{f_n\}}$ represents the effective set of indices of query-key pairs for which we need to calculate the dot product in a given attention head A_i.

Several dilation sequences have been studied in both vision and language transformer architectures. Most commonly, [12, 5, 69, 26] considered dilation sequences, $(f_n)_n = (cn)_{n \in \mathbb{N}}$ that are multiples of a constant factor, $c \in \mathbb{N}$, corresponding to sliding windows with constant dilation factor c. While providing a certain level of efficiency, their attention complexity only reduces from $O(Nw)$ to $O(Nw/c)$, which is still of order N^2 if the window size, W is chosen to be $w = O(N)$. On the other hand, choosing a small window size, $w = O(1)$ prevents the inclusion of any global interactions. Dilation patterns based on different dilation sequences have been less explored; [35] studied exponentially dilated sequences giving rise to attention complexities of $O(N \log w) = O(N \log N)$. We refer to our general architecture in Figure 1 (c).

3.2 Fibottention: Diverse Sparse Attention through Wythoff-Fibonacci Dilation Sequences

While support sets derived from exponential dilation sequences lead to sparse attention matrices, it might happen that crucial query-key interactions are not captured by overly sparse patterns, deteriorating the quality of the resulting MHSA representations.

At the same time, limited experimental results in [32, 5, 20] indicate that varying support set patterns across attention heads can improve model performance. Furthermore, state-of-the-art sparse attention mechanisms aim for a delicate balance between covering local and global interactions [5, 68], and do not necessarily include the interactions on the main diagonal of the attention matrix [50].
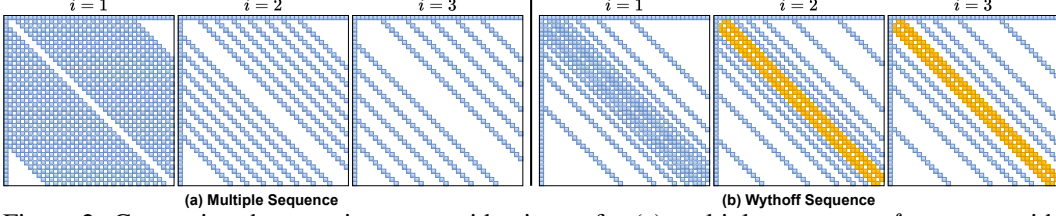
4

Figure 2: Comparing the attention pattern identity ι_Ω for (a) multiples sequence $f_n = c \cdot n$ with multiples, $c = 2, 4, 6$, respectively, and (b) with Wythoff sequence across 3 heads. The central elements in (b), shaded in yellow are only present in the modified Wythoff sequence.

Motivated by these observations, we postulate that *sparse attention matrices with diverse support patterns across attention heads* are desirable and have the potential to be part of efficient transformer architectures, without sacrificing the effectiveness of the learned representation and model accuracy.

Fibonacci Dilation Sequences. We propose a sparse attention pattern that builds crucially on *(generalized) Fibonacci sequences* [52, 31]. The well-known Fibonacci sequence, $(f_n)_{n \in \mathbb{N}}$ is defined as the sequence of integers $(0, 1, 1, 2, 3, 5, 8, 13, \ldots)$ [41] satisfying the linear recurrence relation

$$f_{n+1} = f_n + f_{n-1}, \tag{2}$$

for each $n \geq 2$, where $f_1 = 0$ and $f_2 = 1$. Binet's formula [31] states that the n-th Fibonacci number satisfies $f_n = (\phi^{n-1} - \psi^{n-1})/\sqrt{5}$, where $\phi = (1 + \sqrt{5})/2 \approx 1.618$ is the golden ratio and $\psi = (1 - \sqrt{5})/2$. From this formula, it can be inferred that after initial slow growth, the sequence grows eventually exponentially with respect to the base ϕ.

Similar integer sequences can be defined from the recurrence (2) by fixing the initial elements, $f_1 = a \in \mathbb{N}$ and $f_2 = b \in \mathbb{N}$. Given a window size w, parameters, $a, b \in \mathbb{N}$, and denoting the corresponding *generalized Fibonacci sequence*, $(f_n)_n$ by $\mathrm{Fib}(a, b)$, we can define a corresponding support set for an $N \times N$ attention matrix as $\Omega_w^{\mathrm{Fib}(a,b)} = \{(j, k) \in \{1, \ldots, N\}^2 : |j - k| \in \mathrm{Fib}(a, b), |j - k| \leq w\}$. An experimental ablation study (see Section 4.2) indicates that a simple Fibonacci attention pattern can already be advantageous compared to other dilation sequences.

Wythoff Array and its Properties. Among integer sequences based on order-2 linear recurrence relations, generalized Fibonacci sequences are attractive for creating attention support sets since by varying a and b, a variety of integer values can be covered while retaining the same long-term growth rate (see Lemma 1) as the Fibonacci numbers. Accordingly, we consider the usage of h different Fibonacci-type sequences, $\mathrm{Fib}(a_i, b_i)$ with different initial values $a_1, \ldots, a_h \in \mathbb{N}$ and $b_1, \ldots, b_h \in \mathbb{N}$, giving rise to *head-specific* attention support sets. Defining also head-specific window sizes, $w_1, \ldots, w_h \leq N$, we obtain the support set Ω_i for the i-th attention head matrix A_i defined as $\Omega_{w_i}^{\mathrm{Fib}(a_i, b_i)}$ for each head index $i = 1, \ldots, h$.

Within this framework, we aim to choose the sequence parameters, $\{a_i\}_i$ and $\{b_i\}_i$ such that the following three *desiderata* are satisfied: (*i*) the overlap between different attention head support sets should be minimized, allowing for a semantic specialization of the corresponding head weights during training, (*ii*) the union, $\cup_{i=1}^h \Omega_{w_i}^{\mathrm{Fib}(a_i, b_i)}$ of support sets should be small to retain efficiency, but within that constraint, (*iii*) as many *relevant* query-key interactions as possible should be captured by at least one attention head.

A suitable, essentially hyperparameter-free choice can be derived from the Wythoff array [40, 14, 9], which had been originally introduced in the context of a combinatorial game [65]. The Wythoff array can be considered as a collection of generalized Fibonacci sequences $\{\mathrm{Fib}(a_i, b_i)\}_{i \in \mathbb{N}}$ with specific choices a_i^{Wyt} and b_i^{Wyt} for each $i \in \mathbb{N}$ that have provably *no overlap*, but contain each integer exactly once [40, 14]. In particular, the i-th row sequence of the Wythoff array is given by the sequence, $\mathrm{Fib}(a_i^{\mathrm{Wyt}}, b_i^{\mathrm{Wyt}})$ with initial elements, $a_i^{\mathrm{Wyt}} = \lfloor \lfloor i\phi \rfloor \rfloor$ and $b_i^{\mathrm{Wyt}} = \lfloor \lfloor i\phi \rfloor \phi^2 \rfloor$; see Table 1.

Table 1: Generalized Fibonacci sequences $\mathrm{Fib}(a_i, b_i)$ used by the i-th head's support set Ω_i of Fibottention.

$a_i^{\mathrm{Wyt\text{-}m}}$	$b_i^{\mathrm{Wyt\text{-}m}}$	a_i^{Wyt}	b_i^{Wyt}			
0	1	1	2	3	5	8
1	3	4	7	11	18	29
2	4	6	10	16	26	42
3	6	9	15	24	39	63
4	8	12	20	32	52	84

5

Fibottention. Based on the above considerations, we define a general, novel, sparse attention mechanism, called *Fibottention*, that is designed as a drop-in replacement of full self-attention in multi-head self-attention blocks.

In any given MHSA layer with h heads, for a given head index $i \in [h]$, we restrict the computation of unnormalized attention weights in $A_i \in \mathbb{R}^{N \times N}$ to the support set

$$\Omega_i := \Omega_{w_i}^{\mathrm{Fib}(a_i^{\mathrm{Wyt}}, b_i^{\mathrm{Wyt}})} = \left\{ (j,k) : |j - k| \in \mathrm{Fib}(a_i^{\mathrm{Wyt}}, b_i^{\mathrm{Wyt}}), |j-k| \le w_i \right\}, \qquad (3)$$

where the window size w_i of the i-th head is based on two model-wide hyperparameters $w_{\min}$ and $w_{\max}$, which are chosen based on insights into the modality of the task and the data distribution. Specifically, we choose w_i based on the formula, $w_i = w_{\min} + \left\lfloor \frac{w_{\max} - w_{\min}}{h-1}(i-1) \right\rfloor$ for $i = 1, \ldots, h$, which linearly interpolates between $w_{\min} \le N$, the *minimal window size bound across heads*, and the *maximal window size bound across heads* $w_{\max}$ satisfying $w_{\min} \le w_{\max} \le N$. The resulting *spacing* of window sizes across heads is designed to further diversify the representations learned across heads as, in the case of a large disparity between $w_{\min}$ and $w_{\max}$, heads with lower indices i are biased to learn to encode more local information, whereas heads with $w_i \approx w_{\max}$ are biased towards incorporating more global interactions. Following (1), we define the resulting sparse attention matrix as $A_i^{\Omega_i} = A_i \odot \iota_{\Omega_i}$.

For transformer architectures with several MHSA layers, we further require that the head-wise support sets are shuffled along the layer so that the i-th head uses the sets, $\{\Omega_{\pi(1)}, \ldots, \Omega_{\pi(h)}\}$ within Fibottention, where $\pi : [h] \to [h]$ is a random permutation function (fixed for each layer). We refer to Appendix B for a formal outline.

Fibottention Based on Modified Wythoff Array. While we observed excellent performance of vanilla Fibottention in image classification tasks (see Section 4.1), its performance degrades in tasks in other domains due to its high degree of sparsity, which might not always capture well enough important local interactions. For such cases, we propose a variant of this sparse attention mechanism that *includes two predecessor sequence elements* into each Wythoff row sequence $\mathrm{Fib}(a_i^{\mathrm{Wyt}}, b_i^{\mathrm{Wyt}})$; following the recurrence (2), we can define new initial sequence elements $b_i^{\mathrm{Wyt\text{-}m}} = b_i^{\mathrm{Wyt}} - a_i^{\mathrm{Wyt}}$ and $a_i^{\mathrm{Wyt\text{-}m}} = a_i^{\mathrm{Wyt}} - b_i^{\mathrm{Wyt\text{-}m}}$ and support sets $\Omega_i = \Omega_{w_i}^{\mathrm{Fib}(a_i^{\mathrm{Wyt\text{-}m}}, b_i^{\mathrm{Wyt\text{-}m}})}$ for each head index i. Unlike the original Wythoff array, it is not the case anymore that the resulting sequences contain each integer only at most once [40, 14]; on the other hand, it can be guaranteed that this modified Fibottention shares each query-key interaction pair only across at most *three* heads [14]. The differences in the resulting support set patterns are visualized in Figure 2 and Table 1. We refer to Appendix B for a comprehensive outline that includes both variants of Fibottention. A pseudo-code of Fibottention using Wythoff and modified Wythoff is provided in Appendix B.

In the supplementary material, we provide a proof that the head-wise computational effort for both the standard and the modified variants of Fibottention requires the computation of only $O(N \log(w_{\max}))$ dot products; see Lemma 2.

4 Experiments: Fibottention for Image Classification

In this experiment, we evaluate the effectiveness of Fibottention across various image classification tasks, demonstrate its robustness with different Vision Transformers (ViTs), and perform ablations to justify the design choices of Fibottention.

Datasets. For image classification tasks, we use CIFAR-10 (C10) [33], CIFAR-100 (C100) [33] and ImageNet-1K (IN-1K) [18]. Additionally, we utilize a tiny version of IN-1K, referred to as Tiny ImageNet (Tiny-IN), which consists of 200 classes sampled from the IN-1K dataset. For evaluation, we report the Top-1 image classification accuracy for all the datasets.

Training. For training Fibottention with ViTs, we use the training recipe of DeiT [56]. All our models are trained from *scratch* using ViT-Base (ViT-B) unless otherwise stated. The hyper-parameters $w_{\min}$ and $w_{\max}$ in Fibottention are set to 5 and 65 respectively, unless otherwise stated. Note that we add all class token interactions to the Ω_i in our Fibottention implementation. All the models are trained for 100 epochs with an effective size of 64 using 4 A6000 mid-grade GPUs. Note that for C10 and C100, the input images are resized from 32×32 to 224×224 before being fed to the ViTs.

Table 2: ViT-B, BigBird, and Fibottention for image classification.

Method	C10	C100	Tiny-IN	IN-1K
ViT-B	83.5	59.3	71.9	**75.5**
+BigBird	86.3	62.6	71.0	71.5
+Fibottention	**89.5**	**64.9**	**74.1**	74.2

Table 3: Exploring the robustness of Fibottention (Ours) incorporated into different ViT variants for image classification.

Dataset	ViT-B [56]		ViT-T [56]		Swin-B [37]		CVT-B [63]	
	Vanilla	**+Ours**	Vanilla	**+Ours**	Vanilla	**+Ours**	Vanilla	**+Ours**
C10	83.5	**89.5**	75.4	**76.5**	**81.2**	80.9	**91.4**	91.2
C100	59.3	**64.8**	53.4	**54.0**	**61.0**	60.4	**67.5**	67.3

4.1 Results

Table 2 presents a comparison of Fibottention with representative baselines, namely Vanilla ViT [56] and BigBird [68]. We adapt BigBird within ViTs using sliding window attention with a width $w = 4$. In contrast to NLP applications, where $w = 1$ is approximately 192 for an input sequence of 1024, we find that $w = 4$ is an optimal choice for vision tasks. Fibottention consistently outperforms Vanilla ViT by +7.1%, +9.4% and +3% on the C10, C100, and Tiny-IN datasets respectively by masking 98% of the self-attention head interaction pairs. Also, ViT integrated with Fibottention performs on par with the baseline ViT on the large-scale IN-1K dataset, while significantly outperforming BigBird. This demonstrates that ViTs use redundant information across self-attention matrices $\{A_i\}_{i=1}^h$, and that only 2% of token-token interactions are sufficient and effective for visual representation learning. The accuracy improvements obtained by Fibottention in these datasets are attributed to the inductive bias introduced into the ViTs by localizing the attention head matrices $\{A_i\}_{i=1}^h$ within a range of their diagonal elements, with a maximum offset of $w_{\max} = 65$, and the diversity of learned representations through disjoint masking.

In Table 3, we present the results of Fibottention implemented within various ViT architectures: ViT-Base (ViT-B), ViT-Tiny (ViT-T), Swin base [37] (Swin-B), and CVT base [63] (CVT-B). The improvement in ViT-T is less pronounced compared to ViT-B, attributed to ViT-T's lower embedding dimension and reduced parameterization. Despite Swin and CVT incorporating inductive biases through token merging and convolutional operations, respectively, Fibottention achieves performance on par with their base models by masking substantial key-query pairs of attention values, respectively. This shows the robustness of Fibottention across different ViT variants.

4.2 Ablation Studies

In this section, we illustrate the effectiveness of each design choice in Fibottention on C10 and C100.

Exploring different window sizes. In Figure 3, we plot the classification accuracies of ViT-B modified by Fibottention for different choices of the window size hyperparameters $w_{\min}$ and $w_{\max}$. We observe that incorporating local information by increasing $w_{\min} = w_{\max} = 1$ to 20, which results in $w_i = w_{\min} = w_{\max}$ being fixed across all the heads, enhances classification accuracy. However, extending the interaction to more distant tokens results in a decrease in accuracy. Interestingly, our findings suggest that the token representations learned with varying window sizes are complementary and specific to their locality. This is further confirmed by an experiment where a test sample prediction is deemed accurate if at least one model correctly predicts the ground truth. This approach achieves a maximum accuracy of 94.1%, indicating that each window size contributes unique and complementary information to the token representations in ViTs.

Selecting dilation patterns to compute attention. In Table 4, we explore various options for alternative dilation sequences $(f_n)_n$ (with window size $w_i = w_{\min} = w_{\max} = N/3$ for all attention heads) including the popular powers of 2 [35], for selecting diagonal indices Ω_i via (3), if we *fix* the sequence across all heads. Our findings reveal that the (standard) Fibonacci sequence Fib$(1, 1)$ emerged as the most effective option. This can be attributed to its slow progression, which facilitates a greater focus on local interactions while still incorporating a limited extent of global information.
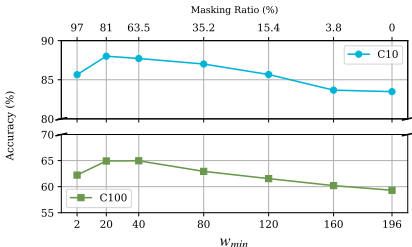

Figure 3: Different window sizes.

Table 4: Ablation of sequence functions.

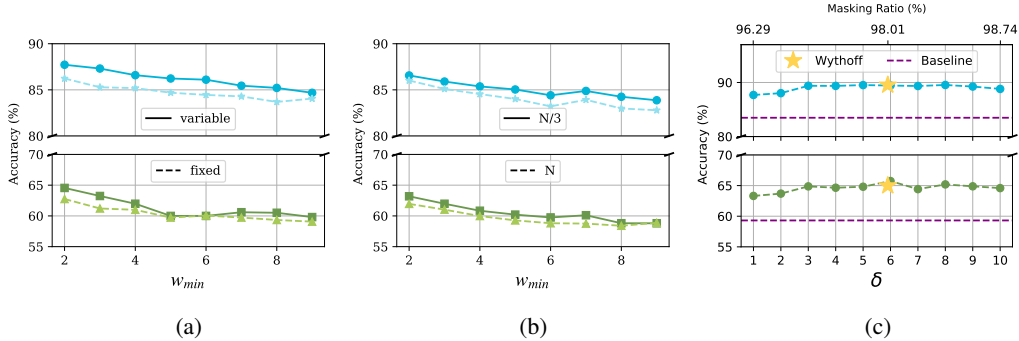| Sequences	CIFAR-10	CIFAR-100
Powers of 2 (2^n for $n \in \mathbb{N}$)	86.1	61.6
Powers of 3 (3^n for $n \in \mathbb{N}$)	85.3	60.2
Square series (n^2 for $n \in \mathbb{N}$)	85.8	61.5
Cube series (n^3 for $n \in \mathbb{N}$)	84.6	59.1
Standard Fibonacci Fib$(1, 1)$	**87.3**	**63.2**

Figure 4: Ablation study of (a) impact of dilation with sequences $(f_n)_{n \in \mathbb{N}} = (c \cdot n)_{n \in \mathbb{N}}$ (multiples of c) fixed (dashed lines) and variable (continuous lines) across heads where $w_i = 5h_i$ and $h \in \{1, \ldots, 12\}$, (b) choice of $w_{\max}$ with sequences $(f_n)_{n \in \mathbb{N}} = \mathrm{Fib}(w_{\min}, 2 \cdot (w_{\min}))$ where $w_{\max} = N$ (dashed lines) and $w_{\max} = N/3$ (continuous lines) fixed across all heads, and (c) with variable dilation sequences such that $\mathrm{Fib}(i + \delta, i + \delta)$ for the i-th head where $i \in \{1, \ldots, 12\}$, with varying δ, vs. Wythoff. The blue and green lines indicate the performance on C10 and C100 respectively.

Impact of dilation. In Figure 4a, we present a plot of *accuracy* versus $w_{\min}$ for Fibottention using a sequence of multiple of $w_{\min}$ fixed across all heads (indicated by dotted lines) and using constant offsets in the sequence, which vary across different heads (indicated by solid lines). We observe that employing varied dilated sequences in computing the attention matrix across different heads enhances the diversity of the heads, thereby enabling the capture of complementary local information in ViTs even with a higher masking ratio; for $w_{\min} = 2$, the masking ratio is 85.5% compared to 72.8% in experiments with fixed sequences across heads.

Choice of $w_{\max}$. In Figure 4b, we present the *accuracy* versus $w_{\min}$ for Fibottention using $w_{\max} = N/3$ and N. Our findings indicate that the hyper-parameter $w_{\max} = N/3$ is optimal, as the regions of interest in image classification tasks are typically confined to localized areas within the image space. Consequently, interactions with distant tokens can introduce noise to the representation of relevant objects in the images, thus $w_{\max} = N/3$ helps focus attention on more pertinent token interactions.

Why Wythoff? In Figure 4c, we present the *accuracy* versus δ, where δ represents the shift in the initial sequence values of $\mathrm{Fib}(i + \delta, i + \delta)$ of the attention support of the i-th head. The window hyperparameters are fixed at $w_{\min} = 5$ and $w_{\max} = N/3$. Interestingly, by employing Wythoff Fibonacci sequences, which encapsulate the maximum non-overlapping token interactions across heads for computing the attention matrix, we achieve the maximum accuracy. This approach eliminates the need for the extra hyperparameter δ, simplifying the model configuration while maintaining performance.

5 Experiments: Fibottention in Other Visual Domains

To demonstrate the generalizability of Fibottention, we integrate it into ViTs designed for other visual perception tasks such as video classification and robot learning.

5.1 Fibottention for Video Action Classification

Datasets. We evaluate Fibottention using three action recognition datasets: Toyota Smarthome [16], Northwestern-UCLA Multiview Activity 3D (NUCLA) [59], and NTU RGB+D (NTU) [48]. The Toyota Smarthome dataset comprises ∼16K videos across 31 classes. For evaluation, we adhere to the cross-subject (CS) protocol and the cross-view (CV2) protocol. The NUCLA dataset consists of ∼1.2K video clips with subjects performing 10 different action classes. The NTU dataset includes 57K videos of 60 actions. Our experiments on NUCLA and NTU datasets utilize the cross-subject (CS) protocol. We report the top-1 action classification accuracy for all the datasets.

Training. For this experiment, we employ the divided-space-time attention variant of TimeSformer [6] for action classification. We integrate Fibottention into the spatial attention module of TimeSformer, considering that the temporal attention module already processes dense attention across the same patch in contiguous frames. For the implementation of Fibottention, we use both its Wythoff and modified Wythoff variants. The hyper-parameters for Fibottention are set to $w_{\min} = 1$ and $w_{\max} = 196$

Table 5: Showcasing Fibottention's performance in video action classification on the Smarthome, NUCLA, and NTU datasets. Top-1 accuracy is reported.

| Method | SmartHome [16] | | NUCLA [59] | NTU [48] |
	CS	CV2	CS	CS
TimeSformer [6]	52.2	36.6	32.9	**74.8**
+BigBird	51.4	40.1	50.9	73.2
+ Fibottention (Wythoff)	55.6	38.6	49.3	69.4
+ Fibottention (Wythoff modified)	**57.1**	**42.3**	**59.6**	73.7

except for NTU where $w_{\max} = 65$. Given that the TimeSformer architecture fundamentally resembles a ViT-B with additional attentional modules, it is initialized with IN-1K pre-trained weights. All video models are trained with a batch size of 32 for 15 epochs. For the Toyota Smarthome dataset, we process video clips of size $8 \times 224 \times 224$ with a sampling rate of 1/32, while for the NUCLA and NTU datasets, we use video clips of size $16 \times 224 \times 224$ with a sampling rate of 1/4.

Results. In Table 5, we compare the action classification results using TimeSformer and other attention mechanisms (BigBird, and Fibottention) integrated within TimeSformer. We observe that Fibottention with modified Wythoff instantiation outperforms all baselines on the Smarthome and NUCLA protocols, utilizing a masking percentage of 94%. Fibottention with modified Wythoff facilitates increased local interactions among query-key pairs compared to the original Wythoff sequences, albeit at the expense of a reduced masking ratio (by 1.5%). The modified Wythoff proves essential in our video experiments, where capturing the temporal evolution of local patches is critical for learning discriminative spatiotemporal representations. On the NTU dataset, TimeSformer integrated with Fibottention performs comparably to the baseline while requiring only 6% of token interactions across the attention head matrices. This finding aligns with observations from IN-1K image experiments, owing to the availability of large-scale training videos in this dataset. Additionally, we find that setting $w_{\max} = N/3$, where N is the number of spatial tokens per frame, yields better results on the NTU dataset than $w_{\max} = N$. We hypothesize that a reason for this is that NTU, similar to image datasets, is a laboratory dataset where the regions of interest are confined within localized areas. Consequently, restricting the upper bound $w_{\max}$ of Fibottention minimizes the introduction of noisy interactions with background tokens. This restriction is not applicable for datasets like NUCLA and Smarthome, where subjects may appear anywhere in the video performing actions.
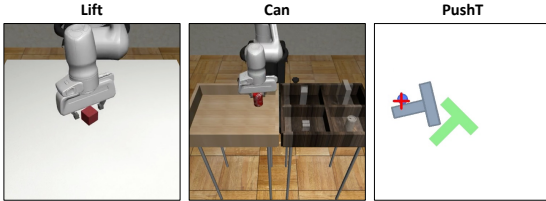

Figure 5: The datasets used in robotics experiments.

Table 6: Performance of Fibottention on behavioral cloning for robotics. The average task completion accuracy is reported.

Visual Backbone	Lift	Can	PushT
ViT-B	0.980	0.960	0.678
+ BigBird	1.000	0.880	0.690
+ Fibottention (Wythoff)	0.820	0.940	0.630
+ Fibottention (Wythoff Modified)	**1.000**	**0.960**	**0.720**

5.2 Fibottention for Robot Learning

Datasets. For robotics experiments, we assess the performance of Fibottention for behavioral cloning [23] in which we aim to learn a robot policy by training a model on state-action pairs obtained from human examples. We evaluate three datasets: Can and Lift from Robomimic [39], and PushT from Implicit Behaviour Cloning [23]. In Lift, the robot must lift up a cube to a specific height. In Can, the robot must move a can into a box. In PushT, the robot must align a T-shaped block with a T-shaped outline. We provide visuals of all three datasets in Figure 5.

Training. Building upon the Crossway Diffusion [36] framework, we modify the architecture by substituting the ResNet visual backbone with a ViT [21], and replace the standard ViT self-attention layers with Fibottention. We employ a batch size of 64 and utilize the base variant of ViT with a patch size of 8 as the visual backbone. For all other hyper-parameters, including the number of training epochs, we follow [36].

Results. We report the average task completion accuracy in Table 6 and find that Fibottention with modified Wythoff instantiation leads to improvements over both the baseline ViT and ViT with BigBird attention, demonstrating the robustness of Fibottention. These observations are consistent with those in our experiments on video action classification.

6   Conclusion

This paper introduces Fibottention, an efficient, robust, and sparse mechanism that diversifies attention computation across heads while maintaining structured sparsity. We further designed two variants of Fibottention — one is effective for image classification tasks (Wythoff), and the other is effective in video domains for action classification and robot imitation learning (modified Wythoff). We used Fibottention in conjunction with multiple state-of-the-art transformer architectures fabricated for visual representation learning. Finally, we experimented Fibottention across three diverse visual tasks, outperforming the baselines on small-scale and mid-scale datasets and performing on par with the baseline on large-scale datasets while utilizing only 2-5% token interaction to compute the multi-headed self-attention. We envision the next generation ViTs [55] using billions of input tokens should use such optimized architectures for efficient training. The limitation of Fibottention lies in its marginally reduced performance on large-scale datasets compared to its baseline. Future work will focus on strategies to recover the compromised accuracy on large-scale data distribution and efforts will be directed towards optimizing Fibottention's sparse implementation as CUDA kernels for enhanced computational efficiency.

Acknowledgements

References

[1] Abhinav Agarwalla, Abhay Gupta, Alexandre Marques, Shubhra Pandit, Michael Goin, Eldar Kurtic, Kevin Leong, Tuan Nguyen, Mahmoud Salem, Dan Alistarh, et al. Enabling High-Sparsity Foundational Llama Models with Efficient Pretraining and Deployment. *arXiv preprint arXiv:2405.03594*, 2024.

[2] Meta AI. Introducing Meta Llama 3: The most capable openly available LLM to date. https://ai.meta.com/blog/meta-llama-3/.

[3] Joshua Ainslie, Santiago Ontanon, Chris Alberti, Vaclav Cvicek, Zachary Fisher, Philip Pham, Anirudh Ravula, Sumit Sanghai, Qifan Wang, and Li Yang. ETC: Encoding Long and Structured Inputs in Transformers. In *Proceedings of the 2020 Conference on Empirical Methods in Natural Language Processing*, pages 268–284, 2020.

[4] Mauricio A Alvarez, Lorenzo Rosasco, Neil D Lawrence, et al. Kernels for vector-valued functions: A review. *Foundations and Trends® in Machine Learning*, 4(3):195–266, 2012.

[5] Iz Beltagy, Matthew E. Peters, and Arman Cohan. Longformer: The long-document transformer. *ArXiv*, abs/2004.05150, 2020.

[6] Gedas Bertasius, Heng Wang, and Lorenzo Torresani. Is space-time attention all you need for video understanding? In *Proceedings of the International Conference on Machine Learning (ICML)*, 2021.

[7] Tom Brown, Benjamin Mann, Nick Ryder, Melanie Subbiah, Jared D Kaplan, Prafulla Dhariwal, Arvind Neelakantan, Pranav Shyam, Girish Sastry, Amanda Askell, et al. Language models are few-shot learners. *Advances in Neural Information Processing Systems (NeurIPS)*, 33:1877–1901, 2020.

[8] Nicolas Carion, Francisco Massa, Gabriel Synnaeve, Nicolas Usunier, Alexander Kirillov, and Sergey Zagoruyko. End-to-end object detection with transformers. In *Proceedings of the European Conference on Computer Vision (ECCV)*, pages 213–229, 2020.

[9] Eric Chen, Adam Ge, Andrew Kalashnikov, Tanya Khovanova, Ella Kim, Evin Liang, Mira Lubashev, Matthew Qian, Rohith Raghavan, Benjamin Taycher, et al. Generalizing the Wythoff Array and other Fibonacci Facts to Tribonacci Numbers. *arXiv preprint arXiv:2211.01410*, 2022.

[10] Ting Chen, Simon Kornblith, Kevin Swersky, Mohammad Norouzi, and Geoffrey E Hinton. Big self-supervised models are strong semi-supervised learners. *Advances in Neural Information Processing Systems (NeurIPS)*, 33:22243–22255, 2020.

[11] Xuanyao Chen, Zhijian Liu, Haotian Tang, Li Yi, Hang Zhao, and Song Han. Sparsevit: Revisiting activation sparsity for efficient high-resolution vision transformer. In *IEEE/CVF Conference on Computer Vision and Pattern Recognition (CVPR)*, 2023.

[12] Rewon Child, Scott Gray, Alec Radford, and Ilya Sutskever. Generating long sequences with sparse transformers. *arXiv preprint arXiv:1904.10509*, 2019.

[13] Kevin Clark, Urvashi Khandelwal, Omer Levy, and Christopher D Manning. What Does BERT Look at? An Analysis of BERT's Attention. In *Proceedings of the 2019 ACL Workshop BlackboxNLP: Analyzing and Interpreting Neural Networks for NLP*, pages 276–286, 2019.

[14] John Conway and Alex Ryba. The Extra Fibonacci Series and the Empire State Building. *Mathematical Intelligencer*, 38(1), 2016.

[15] Gonçalo M Correia, Vlad Niculae, and André FT Martins. Adaptively sparse transformers. In *Proceedings of the 2019 Conference on Empirical Methods in Natural Language Processing and the 9th International Joint Conference on Natural Language Processing (EMNLP-IJCNLP)*, pages 2174–2184, 2019.

[16] Srijan Das, Rui Dai, Michal Koperski, Luca Minciullo, Lorenzo Garattoni, Francois Bremond, and Gianpiero Francesca. Toyota smarthome: Real-world activities of daily living. In *International Conference of Computer Vision (ICCV)*, 2019.

[17] Stéphane d'Ascoli, Hugo Touvron, Matthew Leavitt, Ari Morcos, Giulio Biroli, and Levent Sagun. Convit: Improving vision transformers with soft convolutional inductive biases. *arXiv preprint arXiv:2103.10697*, 2021.

[18] Jia Deng, Wei Dong, Richard Socher, Li-Jia Li, Kai Li, and Li Fei-Fei. Imagenet: A large-scale hierarchical image database. In *Conference on Computer Vision and Pattern Recognition (CVPR)*, pages 248–255, 2009.

[19] Jacob Devlin, Ming-Wei Chang, Kenton Lee, and Kristina Toutanova. BERT: Pre-training of Deep Bidirectional Transformers for Language Understanding. In *Proceedings of NAACL-HLT*, pages 4171–4186, 2019.

[20] Jiayu Ding, Shuming Ma, Li Dong, Xingxing Zhang, Shaohan Huang, Wenhui Wang, Nanning Zheng, and Furu Wei. Longnet: Scaling transformers to 1,000,000,000 tokens. *arXiv preprint arXiv:2307.02486*, 2023.

[21] Alexey Dosovitskiy, Lucas Beyer, Alexander Kolesnikov, Dirk Weissenborn, Xiaohua Zhai, Thomas Unterthiner, Mostafa Dehghani, Matthias Minderer, Georg Heigold, Sylvain Gelly, Jakob Uszkoreit, and Neil Houlsby. An image is worth 16x16 Words: Transformers for image recognition at scale. In *International Conference on Learning Representations*, 2020.

[22] Aritra Dutta, Srijan Das, Jacob Nielsen, Rajatsubhra Chakraborty, and Mubarak Shah. Multiview aerial visual recognition (mavrec): Can multi-view improve aerial visual perception? In *Proceedings of the IEEE/CVF Conference on Computer Vision and Pattern Recognition*, pages 22678–22690, 2024.

[23] Pete Florence, Corey Lynch, Andy Zeng, Oscar Ramirez, Ayzaan Wahid, Laura Downs, Adrian Wong, Johnny Lee, Igor Mordatch, and Jonathan Tompson. Implicit behavioral cloning. *Conference on Robot Learning (CoRL)*, 2021.

[24] Rohit Girdhar, Alaaeldin El-Nouby, Mannat Singh, Kalyan Vasudev Alwala, Armand Joulin, and Ishan Misra. Omnimae: Single model masked pretraining on images and videos. *arXiv preprint arXiv:2206.08356*, 2022.

[25] Qipeng Guo, Xipeng Qiu, Pengfei Liu, Yunfan Shao, Xiangyang Xue, and Zheng Zhang. Startransformer. In *Proceedings of the 2019 Conference of the North American Chapter of the Association for Computational Linguistics: Human Language Technologies, Volume 1 (Long and Short Papers)*, pages 1315–1325, 2019.

[26] Ali Hassani and Humphrey Shi. Dilated neighborhood attention transformer. *arXiv preprint arXiv:2209.15001*, 2022.

[27] Ali Hassani, Steven Walton, Jiachen Li, Shen Li, and Humphrey Shi. Neighborhood attention transformer. In *Proceedings of the IEEE/CVF Conference on Computer Vision and Pattern Recognition (CVPR)*, pages 6185–6194, June 2023.

[28] Edward J Hu, Yelong Shen, Phillip Wallis, Zeyuan Allen-Zhu, Yuanzhi Li, Shean Wang, Lu Wang, and Weizhu Chen. Lora: Low-rank adaptation of large language models. *arXiv preprint arXiv:2106.09685*, 2021.

[29] Qiuhong Ke, Mohammed Bennamoun, Senjian An, Ferdous Sohel, and Farid Boussaid. Learning clip representations for skeleton-based 3d action recognition. *IEEE Transactions on Image Processing*, 27(6):2842–2855, June 2018.

[30] Yoon Kim, Carl Denton, Luong Hoang, and Alexander M Rush. Structured attention networks. In *International Conference on Learning Representations*, 2016.

[31] Thomas Koshy. *Fibonacci and Lucas Numbers with Applications*, volume 2. John Wiley & Sons, 2019.

[32] Olga Kovaleva, Alexey Romanov, Anna Rogers, and Anna Rumshisky. Revealing the Dark Secrets of BERT. In *Proceedings of the 2019 Conference on Empirical Methods in Natural Language Processing and the 9th International Joint Conference on Natural Language Processing (EMNLP-IJCNLP)*, pages 4365–4374, 2019.

[33] Alex Krizhevsky, Geoffrey Hinton, et al. Learning multiple layers of features from tiny images. 2009.

[34] Zhenzhong Lan, Mingda Chen, Sebastian Goodman, Kevin Gimpel, Piyush Sharma, and Radu Soricut. Albert: A lite bert for self-supervised learning of language representations. In *International Conference on Learning Representations*, 2020.

[35] Shiyang Li, Xiaoyong Jin, Yao Xuan, Xiyou Zhou, Wenhu Chen, Yu-Xiang Wang, and Xifeng Yan. Enhancing the locality and breaking the memory bottleneck of transformer on time series forecasting. *Advances in Neural Information Processing Systems*, 32, 2019.

[36] Xiang Li, Varun Belagali, Jinghuan Shang, and Michael S. Ryoo. Crossway diffusion: Improving diffusion-based visuomotor policy via self-supervised learning. In *IEEE International Conference on Robotics and Automation (ICRA)*, 2024.

[37] Ze Liu, Yutong Lin, Yue Cao, Han Hu, Yixuan Wei, Zheng Zhang, Stephen Lin, and Baining Guo. Swin transformer: Hierarchical vision transformer using shifted windows. In *International Conference of Computer Vision (ICCV)*, 2021.

[38] Ze Liu, Yutong Lin, Yue Cao, Han Hu, Yixuan Wei, Zheng Zhang, Stephen Lin, and Baining Guo. Swin transformer: Hierarchical vision transformer using shifted windows. In *Conference on Computer Vision and Pattern Recognition (CVPR)*, pages 10012–10022, 2021.

[39] Ajay Mandlekar, Danfei Xu, Josiah Wong, Soroush Nasiriany, Chen Wang, Rohun Kulkarni, Li Fei-Fei, Silvio Savarese, Yuke Zhu, and Roberto Martín-Martín. What matters in learning from offline human demonstrations for robot manipulation. In *arXiv preprint arXiv:2108.03298*, 2021.

[40] David R Morrison. A Stolarsky array of Wythoff pairs. *A Collection of Manuscripts Related to the Fibonacci Sequence*, 38:134–136, 1980.

[41] The Fibonacci Numbers. Entry A000045: The On-Line Encyclopedia of Integer Sequences `https://oeis.org/A000045`.

[42] Zheng Qu, Liu Liu, Fengbin Tu, Zhaodong Chen, Yufei Ding, and Yuan Xie. Dota: detect and omit weak attentions for scalable transformer acceleration. In *Proceedings of the 27th ACM International Conference on Architectural Support for Programming Languages and Operating Systems*, pages 14–26, 2022.

[43] Alec Radford, Karthik Narasimhan, Tim Salimans, Ilya Sutskever, et al. *Improving language understanding by generative pre-training*. OpenAI, 2018.

[44] Alec Radford, Jeffrey Wu, Rewon Child, David Luan, Dario Amodei, Ilya Sutskever, et al. Language models are unsupervised multitask learners. *OpenAI blog*, 1(8):9, 2019.

[45] Prajit Ramachandran, Niki Parmar, Ashish Vaswani, Irwan Bello, Anselm Levskaya, and Jonathon Shlens. Stand-alone self-attention in vision models. *Advances in Neural Information Processing Systems*, 32, 2019.

[46] Brendan C Reidy, Mohammadreza Mohammadi, Mohammed E Elbtity, and Ramtin Zand. Efficient deployment of transformer models on edge TPU accelerators: A real system evaluation. In *Architecture and System Support for Transformer Models*, 2023.

[47] Dominick Reilly and Srijan Das. Just add π! pose induced video transformers for understanding activities of daily living. In *Proceedings of the IEEE/CVF Conference on Computer Vision and Pattern Recognition*, pages 18340–18350, 2024.

[48] Amir Shahroudy, Jun Liu, Tian-Tsong Ng, and Gang Wang. NTU RGB+D: A Large Scale Dataset for 3D Human Activity Analysis. In *Conference on Computer Vision and Pattern Recognition (CVPR)*, June 2016.

[49] Jinghuan Shang, Kumara Kahatapitiya, Xiang Li, and Michael S Ryoo. Starformer: Transformer with state-action-reward representations for visual reinforcement learning. In *European conference on computer vision*, pages 462–479. Springer, 2022.

[50] Han Shi, Jiahui Gao, Xiaozhe Ren, Hang Xu, Xiaodan Liang, Zhenguo Li, and James Tin-Yau Kwok. Sparsebert: Rethinking the importance analysis in self-attention. In *International Conference on Machine Learning*, pages 9547–9557. PMLR, 2021.

[51] Chenyang Si, Weihao Yu, Pan Zhou, Yichen Zhou, Xinchao Wang, and Shuicheng Yan. Inception transformer. *Advances in Neural Information Processing Systems*, 35:23495–23509, 2022.

[52] Laurence Sigler. *Fibonacci's Liber Abaci: a translation into modern English of Leonardo Pisano's book of calculation*. Springer Science & Business Media, 2003.

[53] Christian Szegedy, Vincent Vanhoucke, Sergey Ioffe, Jon Shlens, and Zbigniew Wojna. Rethinking the inception architecture for computer vision. In *2016 IEEE Conference on Computer Vision and Pattern Recognition (CVPR)*, pages 2818–2826, 2016.

[54] Yi Tay, Mostafa Dehghani, Dara Bahri, and Donald Metzler. Efficient transformers: A survey. *ACM Comput. Surv.*, 55(6):1–28, 2022.

[55] Gemini Team. Gemini: A family of highly capable multimodal models, 2024.

[56] Hugo Touvron, Matthieu Cord, Matthijs Douze, Francisco Massa, Alexandre Sablayrolles, and Herve Jegou. Training data-efficient image transformers & distillation through attention. In *Proceedings of the 38th International Conference on Machine Learning*, volume 139, pages 10347–10357, 2021.

[57] Shikhar Tuli and Niraj K Jha. Edgetran: Device-aware co-search of transformers for efficient inference on mobile edge platforms. *IEEE Transactions on Mobile Computing*, 2023.

[58] Ashish Vaswani, Noam Shazeer, Niki Parmar, Jakob Uszkoreit, Llion Jones, Aidan N Gomez, Łukasz Kaiser, and Illia Polosukhin. Attention is all you need. In *Advances in neural information processing systems*, pages 5998–6008, 2017.

[59] Jiang Wang, Xiaohan Nie, Yin Xia, Ying Wu, and Song-Chun Zhu. Cross-view action modeling, learning, and recognition. In *2014 IEEE Conference on Computer Vision and Pattern Recognition*, pages 2649–2656, June 2014.

[60] Sinong Wang, Belinda Z Li, Madian Khabsa, Han Fang, and Hao Ma. Linformer: Self-attention with linear complexity. *arXiv preprint arXiv:2006.04768*, 2020.

[61] Zhiguo Wang, Patrick Ng, Xiaofei Ma, Ramesh Nallapati, and Bing Xiang. Multi-passage bert: A globally normalized bert model for open-domain question answering. In *Proceedings of the 2019 Conference on Empirical Methods in Natural Language Processing and the 9th International Joint Conference on Natural Language Processing (EMNLP-IJCNLP)*, pages 5878–5882, 2019.

[62] Cong Wei, Brendan Duke, Ruowei Jiang, Parham Aarabi, Graham W Taylor, and Florian Shkurti. Sparsifiner: Learning sparse instance-dependent attention for efficient vision transformers. In *Proceedings of the IEEE/CVF Conference on Computer Vision and Pattern Recognition*, pages 22680–22689, 2023.

[63] Haiping Wu, Bin Xiao, Noel Codella, Mengchen Liu, Xiyang Dai, Lu Yuan, and Lei Zhang. CVT: Introducing convolutions to vision transformers. In *Proceedings of the IEEE/CVF International Conference on Computer Vision*, pages 22–31, 2021.

[64] Kan Wu, Jinnian Zhang, Houwen Peng, Mengchen Liu, Bin Xiao, Jianlong Fu, and Lu Yuan. Tinyvit: Fast pretraining distillation for small vision transformers. In *European Conference on Computer Vision*, pages 68–85. Springer, 2022.

[65] Willem A. Wythoff. A modification of the game of nim. *Nieuw Arch. Wisk*, 7(2):199–202, 1907.

[66] Chulhee Yun, Srinadh Bhojanapalli, Ankit Singh Rawat, Sashank Reddi, and Sanjiv Kumar. Are transformers universal approximators of sequence-to-sequence functions? In *International Conference on Learning Representations*, 2019.

[67] Chulhee Yun, Yin-Wen Chang, Srinadh Bhojanapalli, Ankit Singh Rawat, Sashank Reddi, and Sanjiv Kumar. O (n) connections are expressive enough: Universal approximability of sparse transformers. *Advances in Neural Information Processing Systems*, 33:13783–13794, 2020.

[68] Manzil Zaheer, Guru Guruganesh, Kumar Avinava Dubey, Joshua Ainslie, Chris Alberti, Santiago Ontanon, Philip Pham, Anirudh Ravula, Qifan Wang, Li Yang, et al. Big bird: Transformers for longer sequences. *Advances in Neural Information Processing systems*, 33:17283–17297, 2020.

[69] Pengchuan Zhang, Xiyang Dai, Jianwei Yang, Bin Xiao, Lu Yuan, Lei Zhang, and Jianfeng Gao. Multi-scale vision longformer: A new vision transformer for high-resolution image encoding. In *Proceedings of the IEEE/CVF international conference on computer vision*, pages 2998–3008, 2021.

[70] Zhemin Zhang and Xun Gong. Vision big bird: Random sparsification for full attention. *arXiv preprint arXiv:2311.05988*, 2023.

[71] Xizhou Zhu, Weijie Su, Lewei Lu, Bin Li, Xiaogang Wang, and Jifeng Dai. Deformable DETR: Deformable Transformers for End-to-End Object Detection. In *Proceedings of the International Conference on Learning Representations*, 2020.

Appendix

A Note on Generalized Fibonacci Sequences, the Wythoff Array, and Computational Complexity

To establish a bound on the computational overhead of Fibottention, first, we state a well-known generalization of Binet's formula to generalized Fibonacci sequences, which provides an explicit, non-recursive characterization of the n-th sequence element.

Lemma 1 (Generalized Binet's Formula). *If $Fib(a, b) = (f_n)_{n \in \mathbb{N}}$ is the generalized Fibonacci sequence with initial values $f_1 = a$ and $f_2 = b$, then it holds that*

$$f_n = \frac{b - a\psi}{\sqrt{5}}\phi^{n-1} + \frac{a\phi - b}{\sqrt{5}}\psi^{n-1}$$

for each $n \geq 1$, where $\phi = (1 + \sqrt{5})/2$ and $\psi = (1 - \sqrt{5})/2$.

Now we are set to provide the head-wise computational overhead of the standard and modified variant of Fibottention.

Lemma 2. *Let N be the number of tokens in a multi-head self-attention block. If $(f_n)_n = Fib(1, 1)$ is used as a dilation sequence to create the attention support set $\Omega = \Omega_w^{Fib(1,1)}$ as in 3 for window size w, then the masked attention matrix A^Ω can be computed by evaluating at most*

$$2N(\log(\sqrt{5}w)/\log(\phi) - 1) + 2$$

dot products between query and key vectors, where $\phi = (1 + \sqrt{5})/2$ is the golden ratio.

Proof. Let $(f_1, \ldots, f_d)$ be the Fibonacci indices for one mask. We have $f_{k+1} = f_k + f_{k-1}$. Let $f_1 = a_i$ and $f_2 = b_i$. Let f be the index of the diagonal. Thus the total number of inner products to be computed for the diagonal f is given by $2(N - f)$ considering the symmetric distribution of diagonals in the attention matrix A_i. If we assume a total of D indices for the diagonals $(f_1, \ldots, f_D)$ there exist $2D$ diagonals in the attention matrix A_i the overall computational overhead for self-attention is dependent on D, leading to a total of $\sum_{j=1}^{D} 2(N - f_j)$ computations. We have

$$\sum_{j=1}^{D} 2(N - f_j) = 2DN - 2\sum_{j=1}^{D} f_j \overset{f_{D+2} - f_2 = \sum_{j=1}^{D} f_j}{=} 2DN - 2(f_{D+2} - f_2) \overset{f_{D+2} = w_i}{=} 2DN - 2w_i + 2b_i.$$

Next, we find a bound d on the largest sequence such that $f_d \leq w_i$. We solve for d such that, $f_d \leq w_i$. Using Binet's formula, we obtain:

$$\frac{b - a\psi}{\sqrt{5}}\phi^{d-1} + \frac{a\phi - b}{\sqrt{5}}\psi^{d-1} \leq w_i.$$

We know that $|\Psi| = \frac{1 - \sqrt{5}}{2} \leq 1$. Hence, the sufficient condition for $f_d \leq w_i$ to hold is

$$\frac{b - a\psi}{\sqrt{5}}\phi^{d-1} + \frac{a\phi - b}{\sqrt{5}}1 \leq w_i.$$

Simplifying the above we have

$$d \leq \frac{\log(\sqrt{5}w_i + b - a\phi)}{\log \phi} + 1.$$

Since $\phi = \frac{1 + \sqrt{5}}{2}$ and $a \geq 1$, we have $d \leq \frac{\log(\sqrt{5}w_i + b)}{\log \phi} + 1$. Therefore, the total bound is given by

$$\sum_{j=1}^{D} 2(N - f_j) = 2DN - 2w_i + 2b_i \leq 2N\left(\frac{\log(\sqrt{5}w_i + b)}{\log \phi} + 1 + b - w_i\right).$$

Hence the result.

$\square$

B   Algorithmic Outline for Fibottention

In this section, we provide detailed pseudocode for Fibottention. Algorithm 1 generates the Fibonacci sequence with specific constraints. Algorithm 2 produces non-overlapping sequences across all attention heads. Finally, Algorithm 3 demonstrates how Fibottention can be implemented in Multi-Head Self-Attention (MHSA) to compute the attention mechanism.

Algorithm 1 Generating Fibonacci Sequence with Constraint

1: **Input:** a, b, and w_i
2: **Output:** fib_seq
3: $fib\_seq \leftarrow [a, b]$
4: **while** $fib\_seq[-1] < w_i$ **do**
5:     $next\_num \leftarrow fib\_seq[-1] + fib\_seq[-2]$
6:     $fib\_seq \leftarrow fib\_seq \cup [next\_num]$
7: **end while**
8: **return** fib_seq

Algorithm 2 Pseudocode for generating mask for all heads

1: **Input:** $L, N, w_{\min}, w_{\max}, is\_modified$
2: **Output:** $\Omega \in (0,1)^{h \times (N+1) \times (N+1)}$
3: **Initialize:**
4: $\phi \leftarrow (1 + \sqrt{5})/2$
5: $a \leftarrow \lfloor \lfloor i \times \phi \rfloor \times \phi \rfloor$
6: $b \leftarrow \lfloor \lfloor i \times \phi \rfloor \times \phi^2 \rfloor$
7: **for each** head $i \in \{1, \ldots, h\}$ **do**
8:     $w_i \leftarrow w_{\min} + \lfloor ((i-1) \times (w_{\max} - w_{\min}))/(h-1) \rfloor$
9:     $\Theta \leftarrow (0)^{N \times N}$ ▷ Intermediate tensor to hold the masks without the class token
10:    $I \leftarrow \textbf{getFibonacci}(a, b, w_i)$ ▷ Algorithm 1
11:    **if** $is\_modified$ **and** $i > 1$ **then**
12:        append from $(0, (a - i))$ to I
13:        append from $(0, (i - 1))$ to I
14:    **end if**
15:    **for each** $o \in I$ **do**
16:        **for each** $j \in \{0, \ldots, N - o\}$ **do**
17:            $(\Theta)_{j,j+1} \leftarrow 1$ ▷ Upper triangular matrix
18:        **end for**
19:        **for each** $k \in \{o, \ldots, N\}$ **do**
20:            $(\Theta)_{k+1,k} \leftarrow 1$ ▷ Lower triangular matrix
21:        **end for**
22:    **end for**
23:    $\Omega_i \leftarrow (1)^{(N+1) \times (N+1)}$
24:    **for** $j \in \{1, \ldots, N\}$ **do**
25:        **for** $k \in \{1, \ldots, N\}$ **do**
26:            $(\Omega_i)_{j+1,k+1} \leftarrow (\Theta)_{j,k}$
27:        **end for**
28:    **end for**
29: **end for**
30: $\Omega \leftarrow \Omega_1 \times \Omega_2 \times \ldots \times \Omega_h$
31: $\Omega \leftarrow \text{randomshuffle}(L, \Omega)$ ▷ L is the Layer of Transformer Block
32: **return** Ω

Algorithm 3 Pseudocode for Fiboattention in a single Vision Transformer Block

---

1: **Input:** $X \in \mathbb{R}^{N+1 \times d}$
2: **Output:** $O \in \mathbb{R}^{N+1 \times d}$
3: **Parameters:** $W_i^Q, W_i^K, W_i^V \in \mathbb{R}^{d \times d_h}, d_h = \frac{d}{h}$
4: **HyperParameters:** $w_{\min}, w_{\max}, is\_modified$
5: $\iota_\Omega \leftarrow getMask(L, N, h, w_{\min}, w_{\max}, is\_modified)$ ▷ From Algorithm 2
6: **for each** head $i \in \{1, \ldots, h\}$ **do**
7: $\quad Q_i \leftarrow X \cdot W_i^Q$
8: $\quad K_i \leftarrow X \cdot W_i^K$
9: $\quad V_i \leftarrow X \cdot W_i^V$
10: $\quad A_i \leftarrow Q_i \cdot K_i^T$
11: $\quad \mathcal{A}_i^\Omega \leftarrow \text{sign}(\mathcal{A}_i) \odot (|\mathcal{A}_i| \odot \iota_{\Omega[i,:,:]})$
12: $\quad A_i^\Omega \leftarrow \text{softmax}(A_i^\Omega)$
13: $\quad Z_i \leftarrow (A_i^\Omega \cdot V_i) \in \mathbb{R}^{N+1 \times d_h}$
14: **end for**
15: $Z \in \mathbb{R}^{N+1 \times (h \cdot d_h)}$
16: $O \leftarrow Z \cdot W^Z$, where $W^Z \in \mathbb{R}^{(h \cdot d_h) \times d}$
17: **return** O

C Further Implementation Details

In this section, we provide a comprehensive outline for the implementation of Fibottention within a multi-head self-attention block of a transformer architecture.

C.1 Integration of Fibottention in variants of ViTs

Fibottention is robust and can be easily integrated into various ViTs. For our experiments, we implemented Fibottention in two state-of-the-art ViTs: Swin Transformer [37] and CVT [63].

We have adapted the Swin-B architecture by replacing the self-attention within the windows by Fibottention only in the first two stages of the model. The last two stages of the Swin-B with lower complexity owing to the patch merging modules, remain unmodified. We follow the standard training procedure of Swin-B [38].

ConvVIT-Base(CVT-B) [63] consists of gated positional self-attention(GPSA) and MHSA blocks. We apply Fibottention only in the MHSA blocks. We train CVT-B following [63]. We conducted all these experiments for 100 epochs using a batch size of 64 on 4 RTX A6000 GPUs.

C.2 Experimental Configuration for Image Classificaion

All the experiments performed for Image Classification benchmarking are detailed in 7.

Table 7: CIFAR-10, CIFAR-100, and ImageNet-1K Training Settings [56].

Input Size	224×224
Crop Ratio	0.9
Batch Size	64
Optimizer	AdamW
Optimizer Epsilon	1.0e-06
Momentum	0.9
Weight Decay	0.05
Gradient Clip	1.0
Learning Rate Schedule	Cosine
Learning Rate	1e-3
Warmup LR	1.0e-6
Min LR	1.0e-5
Epochs	100
Decay Epochs	1.0
Warmup Epochs	5
Decay Rate	0.988
Exponential Moving Average (EMA)	True
EMA Decay	0.99992
Random Resize & Crop Scale and Ratio	(0.08, 1.0), (0.67, 1.5)
Random Flip	Horizontal 0.5; Vertical 0.0
Color Jittering	0.4
Auto-agumentation	rand-m15-n2-mstd1.0-inc1
Mixup	True
Cutmix	True
Mixup, Cutmix Probability	0.5, 0.5
Mixup Mode	Batch
Label Smoothing	0.1

D   Further Abaltion Studies of Fibottention

D.1   Visualization of Fibottention

The attention matrix visualizations prior to training in 6a reveal a lack of focus along the diagonals, indicating that the model has not yet learned to direct its attention towards specific image features. In contrast, the visualizations for the baseline model ViT-B in Fig. 6b, after 100 epochs of training, exhibit more defined patterns, with the model concentrating its attention on certain image regions. Conversely, Fibottention, as shown in Fig. 6, appears to concentrate its attention along the diagonals, suggesting an accumulation of information from high token-to-token interactions at a local level.

(a)   (b)   (c)
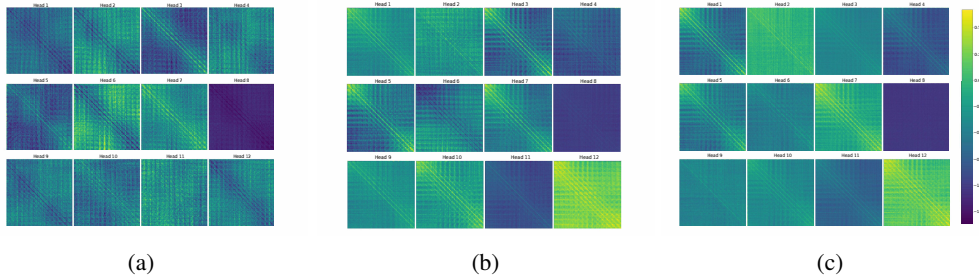
Figure 6: This figure illustrates the visualization of the attention matrix for each head, aggregated over a batch of 64 images. The visualizations are presented for three different scenarios: (a) before training, (b) after the baseline model is trained for 100 epochs, and (c) after training with Fibottention for 100 epochs.

D.2   Impact of principal diagonal for attention computation

In Table 8, we present the image classification performance of Fibottention using a fixed local window for computing attention, both with and without the principal diagonal. Our findings indicate that local token interactions alone are sufficient for learning discriminative token representations. The principal diagonal is not required as it introduces redundant information into the token representations.

Table 8: Comparison on performance with a fixed local window w_i with and without principal diagonal proving that the principal diagonal is not only redundant, it, in turn, harms the performance, proving the claims of SparseBERT [50].

w_i	w/ Main Diagonal			w/o Main Diagonal		
	Mask Ratio	C10	C100	Mask Ratio	C10	C100
2	97.46	86.1	62.0	97.97	85.7	62.2
10	89.57	86.8	62.4	90.08	87.0	63.4
15	84.81	87.5	64.7	85.32	88.0	64.8
20	80.17	87.9	64.9	80.69	88.0	64.9
40	62.94	87.6	64.5	63.45	87.7	65.0